Optik - International Journal for Light and Electron Optics 280 (2023) 170772

Contents lists available at ScienceDirect

Optik - International Journal for Light and Electron Optics

journal homepage: www.elsevier.com/locate/ijleo

Original research article

(Invited) Two-color soliton meta-atoms and molecules

O. Melchert *, S. Willms, I. Babushkin, U. Morgner, A. Demircan

Leibniz Universität Hannover, Institute of Quantum Optics, Welfengarten 1, Hannover, 30167, Germany
Leibniz Universität Hannover, Cluster of Excellence PhoenixD, Welfengarten 1A, Hannover, 30167, Germany

ARTICLE INFO

Keywords:
Nonlinear optics
Optical solitons
Two-color soliton molecules
Resonant radiation

ABSTRACT

We present a detailed overview of the physics of two-color soliton molecules in nonlinear waveguides, i.e. bound states of localized optical pulses which are held together due to an incoherent interaction mechanism. The mutual confinement, or trapping, of the subpulses, which leads to a stable propagation of the pulse compound, is enabled by the nonlinear Kerr effect. Special attention is paid to the description of the binding mechanism in terms of attractive potential wells, induced by the refractive index changes of the subpulses, exerted on one another through cross-phase modulation. Specifically, we discuss nonlinear-photonics meta atoms, given by pulse compounds consisting of a strong trapping pulse and a weak trapped pulse, for which trapped states of low intensity are determined by a Schrödinger-type eigenproblem. We discuss the rich dynamical behavior of such meta-atoms, demonstrating that an increase of the group-velocity mismatch of both subpulses leads to an ionization-like trapping-to-escape transition. We further demonstrate that if both constituent pulses are of similar amplitude, molecule-like bound-states are formed. We show that z-periodic amplitude variations permit a coupling of these pulse compound to dispersive waves, resulting in the resonant emission of Kushi-comb-like multi-frequency radiation.

1. Introduction

The confinement of two – and possibly more – quasi co-propagating optical pulses has been discussed in terms of various propagation settings since the 80's of the last century, with early accounts discussing the self-confinement of multimode optical pulses in glass fibers [1], nonlinear pairing of light and dark optical solitons [2,3], and stability of solitons with different polarization components in birefringent fibers [4]. A very paradigmatic instance of self-confinement is supported by the standard nonlinear Schrödinger equation (NSE) [5,6]. In the integrable case, it features localized field pulses given by solitary waves [7]. When considering two or more quasi group-velocity matched pulses, their incoherent, cross-phase modulation (XPM) induced mutual interaction co-determines their dynamics [1–4,8–11]. For instance, in nonlinear waveguides with a single zero-dispersion point, a soliton induces a strong refractive index barrier that cannot be surpassed by quasi group-velocity matched waves located in a domain of normal dispersion [12], resulting in their mutual repulsion. The underlying interaction process is enabled by a general wave reflection mechanism originally reported in fluid dynamics [13]. In optics this process is referred to as push-broom effect [14], optical event horizon [15,16], or temporal reflection [17]. This interaction mechanism allows for a strong and efficient control of light pulses [18–20], and has been shown to appear naturally during the supercontinuum generation process [21–23]. When considering waveguides that support group-velocity matched propagation of pulses in separate domains of anomalous dispersion, their mutual interaction is expressed in a different way: the aforementioned XPM induces attractive potentials that hold the pulses

* Corresponding author at: Leibniz Universität Hannover, Institute of Quantum Optics, Welfengarten 1, Hannover, 30167, Germany.
E-mail address: melchert@iqo.uni-hannover.de (O. Melchert).

https://doi.org/10.1016/j.ijleo.2023.170772
Received 1 March 2023; Accepted 7 March 2023
Available online 15 March 2023

together, enabling two-color soliton molecules through an incoherent binding mechanism [24]; the resulting pulse compound consists of two subpulses at vastly different center frequencies. Putting emphasis on the frequency-domain representation of these pulse compounds lead to observe that a soliton can in fact act as a localized trapping potential with a discrete level spectrum [24]. Let us emphasize that in order to achieve a strong attractive interaction between the subpulses of such pulse compounds, group-velocity matching is crucial [25]. In terms of a modified NSE with added fourth-order dispersion, these objects where identified as parts of a large family of generalized dispersion Kerr solitons that can be characterized using the concept of a meta-envelope [26]. Such pulses were recently verified experimentally in mode-locked laser cavities [27–29]. In a complementary approach to the multi-scales analysis presented in Ref. [26], modeling both subpulses in terms of coupled NSEs allowed to derive a special class of two-color soliton pairs and their meta-envelopes in closed form [30]. Let us note that the concept of soliton molecules has meanwhile been extended to pulse compounds with three frequency centers [31], and recently also to a number of J equally spaced frequency components [27,32]. Further, two-color soliton microcomb states with similar structure where also observed in the framework of the Lugiato–Lefever equation [33,34]. The underlying scheme is much more general and requires quasi group-velocity matching between different optical pulses. This can be achieved in different settings, and can, e.g., already been found in an early work of Hasegawa [1], where a strong incoherent XPM interaction between different components of a multimode optical pulse has been considered. At this point, we would also like to emphasize that these pulse compounds are different from usual soliton molecules, which can be realized by dispersion engineering in the framework of a standard NSE [35], characterized by two pulses separated by a fixed temporal delay and stabilized by a phase relation between both pulses [36].

Here, we review the rich dynamical behavior of two-color pulse compounds, which consist of two group-velocity matched subpulses in distinct domains of anomalous dispersion, with frequency loci separated by a vast frequency gap. First, we will demonstrate paradigmatic propagation scenarios that demonstrate photonic meta-atoms, arising in the limiting case where the pulse compounds consist of an intense trapping pulse, given by a soliton, and a weak trapped pulse. Then, we will address the case where both subpulses have similar amplitudes, so that their mutual XPM induced confining action results in the formation of a narrow two-color soliton molecule. Finally, we show that non-stationary dynamics of the subpulses results in the emission of resonant radiation, and we show how the location of the newly generated frequencies depends on the z-periodic amplitude and width variations of the oscillating soliton molecule.

The article is organized as follows. In Section 2 we discuss the propagation model used for our theoretical investigations of two-color meta-atoms and soliton molecules, and detail the numerical methods employed for their simulation and analysis. In Section 3 we demonstrate the ability of solitons to act as attractive potential wells that can host trapped states, and probe the stability of the resulting photonic meta-atoms with respect to a group-velocity mismatch between the trapping soliton and the trapped state. In Section 4 we derive a simplified model that yields simultaneous solutions for the subpulses that make up a two-color soliton molecule and show that these solutions entail the two-color soliton pairs derived in Ref. [30]. We perturb these pulse compounds by increasing their initial amplitude, which results in periodic amplitude and width oscillations, and triggers the generation of resonant multi-frequency radiation with a complex structure that can be precisely predicted theoretically. Section 5 concludes with a summary.

2. Model and methods

Propagation model. In order to study the propagation dynamics of nonlinear photonic meta-atoms and two-color soliton molecules, we consider a modified nonlinear Schrödinger equation (NSE) of the form

$$i\partial_z A = \left(\frac{\beta_2}{2}\partial_t^2 - \frac{\beta_4}{24}\partial_t^4\right) A - \gamma|A|^2 A, \tag{1}$$

describing the single-mode propagation of a complex-valued field $A \equiv A(z,t)$, on a periodic temporal domain of extent T for the boundary condition $A(z,-T/2) = A(z,T/2)$. The linear part of Eq. (1) includes higher orders of dispersion, with $\beta_2 > 0$ (in units of $\mathrm{fs}^2/\mu\mathrm{m}$) a positive-valued group-velocity dispersion coefficient, and $\beta_4 < 0$ ($\mathrm{fs}^4/\mu\mathrm{m}$) a negative-valued fourth-order dispersion coefficient. The nonlinear part of Eq. (1) includes a positive-valued scalar nonlinear coefficient γ ($\mathrm{W}^{-1}/\mu m$). Considering the discrete set of angular frequency detunings $\Omega \in \frac{2\pi}{T}\mathbb{Z}$, the transform-pair

$$A_\Omega(z) = \mathsf{F}[A(z,t)] \equiv \frac{1}{T}\int_{-T/2}^{T/2} A(z,t)\, e^{i\Omega t}\, \mathrm{d}t, \tag{2a}$$

$$A(z,t) = \mathsf{F}^{-1}[A_\Omega(z)] \equiv \sum_\Omega A_\Omega(z)\, e^{-i\Omega t}, \tag{2b}$$

specifies a Fourier transform [Eq. (2a)], and the corresponding inverse [Eq. (2b)], relating the field envelope $A(z,t)$ to the spectral envelope $A_\Omega(z)$.

Propagation constant. Using the identity $\partial_t^n\, e^{-i\Omega t} = (-i\Omega)^n\, e^{-i\Omega t}$ of the spectral derivative,[1] the frequency-domain representation of the propagation constant is given by the polynomial expression

$$\beta(\Omega) = \frac{\beta_2}{2}\Omega^2 + \frac{\beta_4}{24}\Omega^4. \tag{3a}$$

[1] Let us note that the "-"-sign in the bracket on the right-hand-side of the preceding identity reflects the sign-choice of the plane-wave basis in Eqs. (2). This has to be taken into account when using scientific computing tools such as, e.g., Python's scipy package [37,38], where readily available routines for spectral derivative exist that implement a different sign-choice for the pair of Fourier-transforms.

The frequency-dependent inverse group-velocity of a mode at detuning Ω reads

$$\beta_1(\Omega) \equiv \partial_\Omega \beta(\Omega) = \beta_2 \Omega + \frac{\beta_4}{6}\Omega^3, \tag{3b}$$

with group-velocity (GV) $v_g(\Omega) = 1/\beta_1(\Omega)$, and the group-velocity dispersion (GVD) is given by

$$\beta_2(\Omega) \equiv \partial_\Omega^2 \beta(\Omega) = \beta_2 + \frac{\beta_4}{2}\Omega^2. \tag{3c}$$

Subsequently, we use the parameter values $\beta_2 = 1\ \mathrm{fs}^2/\mu\mathrm{m}$, and $\beta_4 = -1\ \mathrm{fs}^4/\mu\mathrm{m}$, resulting in the model dispersion characteristics shown in Fig. 1. For the nonlinear coefficient in Eq. (1) we use $\gamma = 1\ \mathrm{W}^{-1}/\mu m$. As evident from Fig. 1(c), the GVD profile Eq. (3c) has a concave downward shape with two zero-dispersion points, defined by the condition $\beta_2(\Omega) \stackrel{!}{=} 0$, located at $\Omega_{Z1,Z2} = \mp\sqrt{2\beta_2/|\beta_4|} = \mp\sqrt{2}\,\mathrm{rad/fs}$. It exhibits anomalous dispersion for $\Omega < \Omega_{Z1}$ as well as for $\Omega > \Omega_{Z2}$. The interjacent frequency range $\Omega_{Z1} < \Omega < \Omega_{Z2}$ exhibits normal dispersion. Inspecting the inverse group velocity shown in Fig. 1(b), it can be seen that two frequencies are GV matched to $\Omega = 0$. Due to the symmetry of the propagation constant, these are given by the pair $\Omega_1 = -\Omega_2 = -\sqrt{6\beta_2/|\beta_4|} \approx -2.828\ \mathrm{rad/fs}$, uniquely characterized by $\beta(\Omega_1) = \beta(\Omega_2)$ and indicated by the open and filled circles in Fig. 1. In fact, for the considered propagation constant, GV matching of three distinct modes can be realized as long as the frequency loci in AD1 and AD2 lie within the range of frequencies shaded in red in Fig. 1(b). Let us note that the type of GV matching for two optical pulses at vastly different center frequencies, supported by the propagation constant Eq. (3a), is methodologically different from the type of GV matching that supports quasi co-propagation of different modes with similar frequencies [1]. Nevertheless, both allow for quasi co-propagation of optical pulses under different circumstances, supporting similar XPM induced propagation effects. In our case, quasi group-velocity matched propagation of optical pulses across a vast frequency gap is possible, enabled by a tailored propagation constant with multiple zero-dispersion points. Further, the considered mechanism of GV matching differs from that in Ref. [39], wherein two pulses at the same central frequency but different polarization states were assumed to be launched in the anomalous dispersion regime of a hollow-core photonic crystal fiber filled with a noble gas. The mathematical structure of Eq. (1) and the above choice of parameters yields a very basic setting supporting the stable propagation of nonlinear photonic meta-atoms and two-color soliton molecules. In fact, the two-parameter GVD curve shown in Fig. 1(c) is a simplified model of the dispersion considered earlier in Ref. [24], wherein two-color soliton molecules were first demonstrated, and is similar to the setting considered in Ref. [26], wherein generalized dispersion Kerr solitons were described comprehensively. However, let us note that the phenomena reported below are not limited to the particular choice of the above parameters and persist even in the presence of perturbations such as pulse self-steepening [25,30], which can be accounted for by replacing $\gamma \to \gamma(\Omega)$ in the nonlinear part of Eq. (1), and – with some reservation – a self-frequency shift caused by the Raman effect [31].

Propagation algorithm. For our pulse propagation simulations in terms of Eq. (1), we employ the "Conservation quantity error" method (CQE) [40,41]. It maintains an adaptive z-propagation stepsize h, and uses a conservation law of the underlying propagation equation to guide stepsize selection. Specifically, we here use the relative error

$$\delta_E(z) = \frac{|E(z+h) - E(z)|}{E(z)}, \tag{4}$$

where E is the total energy, conserved by Eq. (1). Employing Parseval's identity for Eqs. (2) [42,43], the total energy in the time and frequency domains is given by

$$E(z) = \int_{-T/2}^{T/2} |A(z,t)|^2\ \mathrm{d}t = T \sum_\Omega |A_\Omega(z)|^2, \tag{5}$$

with instantaneous power $|A(z,t)|^2$ (W = J/s), and power spectrum $|A_\Omega(z)|^2$ (W). The CQE method is designed to keep the relative error δ_E within the goal error range $(0.1\,\delta_\mathrm{G}, \delta_\mathrm{G})$, for a preset local goal error δ_G (throughout our numerical experiments we set $\delta_\mathrm{G} = 10^{-10}$). This is accomplished by decreasing the stepsize h when necessary while increasing h when possible. To advance the field from position z to $z+h$, the CQE uses the "Fourth-order Runge–Kutta in the interaction picture" (RK4IP) method [44]. The ability of the algorithm to increase or decrease the stepsize is most valuable when the propagation of an initial condition results in a rapid change of the pulse intensities over short propagation distances. Nevertheless, if one is willing to accept an increased running time resulting from an integration scheme with fixed stepsize, usual split-step Fourier methods [43,45,46] will work similarly well.

Spectrograms. To assess the time–frequency interrelations within the field $A(z,t)$ at a selected propagation distance z, we use the spectrogram [47–49]

$$P_S(t,\Omega;z) = \frac{1}{2\pi}\left|\int_{-T/2}^{T/2} A(z,t')h(t'-t)e^{-i\Omega t'}\ \mathrm{d}t'\right|^2. \tag{6}$$

To localize the field in time, we use a hyperbolic-secant window function $h(x) = \mathrm{sech}(x/\sigma)$ with width parameter σ.

Incoherently coupled pulse pairs. To facilitate a simplified description of two-color pulse compounds in the form

$$A(z,t) = A_1(z,t)\,e^{-i\Omega_1 t} + A_2(z,t)\,e^{-i\Omega_2 t}, \tag{7}$$

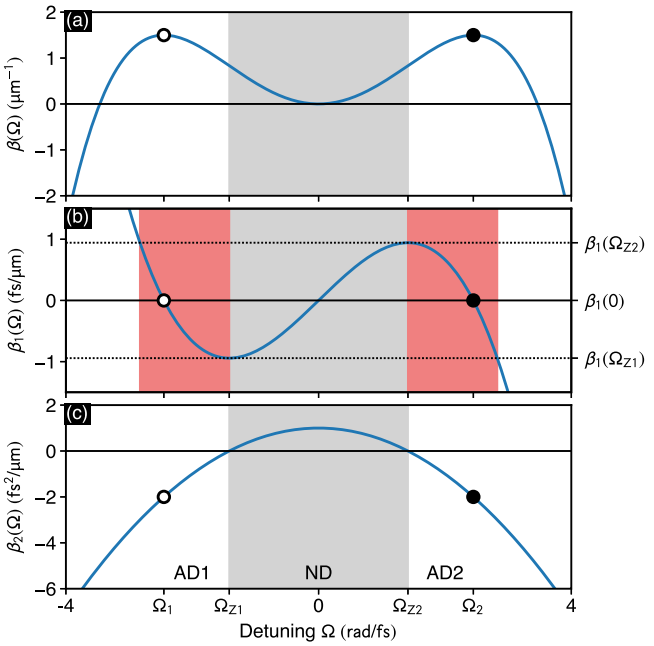

Fig. 1. Details of the frequency-dependent propagation constant supporting nonlinear-photonic meta-atoms and two-color soliton molecules. (a) Propagation constant, (b) inverse group velocity, and, (c) group-velocity dispersion. In (c), AD1 and AD2 label two distinct domains of anomalous dispersion, separated by an extended domain of normal dispersion (labeled ND). In (a–c), the domain of normal dispersion is shaded gray. Zero-dispersion points are labeled Ω_{Z1} and Ω_{Z2}. In (b), the frequency range shaded in red allows for group-velocity matching of two modes with loci in AD1 and AD2. Open circle (labeled Ω_1) and filled circle (labeled Ω_2) indicate such a pair of group-velocity matched frequencies. (For interpretation of the references to color in this figure legend, the reader is referred to the web version of this article.)

in which two quasi group-velocity-matched subpulses $A_1 \equiv A_1(z,t)$ and $A_2 \equiv A_2(z,t)$ exist at the frequency gap $\Omega_{\rm gap} = |\Omega_2 - \Omega_1|$, it is convenient to consider the two coupled nonlinear Schrödinger equations (CNSEs) [6,10,11]

$$i\partial_z A_1 + \beta_0' A_1 - i\beta_1'\partial_t A_1 - \frac{\beta_2'}{2}\partial_t^2 A_1 + \gamma'\left(|A_1|^2 + 2|A_2|^2\right) A_1 = 0, \tag{8a}$$

$$i\partial_z A_2 + \beta_0'' A_2 - i\beta_1''\partial_t A_2 - \frac{\beta_2''}{2}\partial_t^2 A_2 + \gamma''\left(|A_2|^2 + 2|A_1|^2\right) A_2 = 0. \tag{8b}$$

The parameters in Eqs. (8) are related to Eqs. (3) through $\beta_0' = \beta(\Omega_1)$, $\beta_0'' = \beta(\Omega_2)$, $\beta_1' = \beta_1(\Omega_1)$, $\beta_1'' = \beta_1(\Omega_2)$, $\beta_2' = \beta_2(\Omega_1)$, $\beta_2'' = \beta_2(\Omega_2)$, and, $\gamma' = \gamma'' = \gamma$. The mismatch of inverse GV for both subpulses is given by $\Delta\beta_1 \equiv |\beta_1'' - \beta_1'|$. For specific choices of the detunings Ω_1 and Ω_2, exact GV matching, signaled by $\Delta\beta_1 = 0$, can be achieved. In contrast to Eq. (1), the incoherently coupled Eqs. (8) neglect higher-orders of dispersion within their linear parts, as well as rapidly varying four-wave-mixing terms within their nonlinear parts. The mutual interaction of both subpulses is taken into account via XPM. As evident from Eq. (8a), pulse A_1 can be viewed as being exposed to a total potential field of the form $V_1 \equiv \gamma'(|A_1|^2 + 2|A_2|^2)$, entailing the effects of SPM and XPM. Likewise, A_2 is exposed to the potential field $V_2 \equiv \gamma''(|A_2|^2 + 2|A_1|^2)$. As we will show in Section 3, 4, the potential fields V_1 and V_2 yield attractive potentials that enable the mutual trapping of both subpulses. Subsequently we take Ω_1 and Ω_2 as indicated in Fig. 1, so that the above parameters are given by $\beta_0' = \beta_0'' = 1.33\ \mu\text{m}^{-1}$, $\beta_1' = \beta_1'' = 0$, $\beta_2' = \beta_2'' = -2\ \text{fs}^2/\mu\text{m}$, and, $\gamma' = \gamma'' = 1\ \text{W}^{-1}/\mu m$. For a more general description of simultaneous solutions in the form of Eq. (7), we will continue to refer to the nonlinear coefficients in Eqs. (8) as γ' [Eq. (8a)] and γ'' [Eq. (8b)]. In addition, the scalar factors $\beta_0' = \beta_0'' \equiv \beta_0$ can be removed by a common linear transformation $A_{1,2} \to A_{1,2}e^{i\beta_0 z}$, which does not affect the z-propagation dynamics of the interacting pulses.

Let us note that, in general, higher-orders of dispersion within a modified NSE can cause a solitary wave to shed resonant radiation [50], and can result in a modification of its group-velocity [50,51]. These types of perturbations are neglected by Eqs. (8), which can be justified in the limit where the subpulse separation $\Omega_{\rm gap}$ is large and their spectra are sufficiently narrow. Moreover, in case of a frequency dependent coefficient function $\gamma(\Omega)$, $\gamma' = \gamma(\Omega_1)$ and $\gamma'' = \gamma(\Omega_2)$ in Eqs. (8). Let us point out that, in the presence of a linear variation of γ, a solitary wave exhibits a further modification of its group-velocity [52], an effect neglected by Eqs. (8). It is important to bear these perturbation effects in mind when comparing results based on Eqs. (8) to numerical simulations in terms of the full model Eq. (1).

We can relate the above trapping mechanism for two-color pulse compounds to the mechanism enabling the self-confinement of a multimode optical pulses in a multimode fiber, discussed by Hasegawa as early as 1980 [1]. Therein, Hasegawa considered a propagation equation of the nonlinear Schrödinger type for a multimodal pulse, where the nonlinear change of the refractive index, felt by an individual mode, depends on the total intensity of the multimodal pulse. This results in coupled equations for the

different modes, wherein an individual mode perceives the intensity of the total pulse as a potential field. If the considered mode is subject to anomalous dispersion, the potential is attractive. Based on the expectation that if the velocity mismatch between a given mode and the potential is smaller than the escape velocity, the potential has the ability to trap the mode, he derived a condition for self-confinement of the multimode pulse. While the results in Ref. [1] are valid for multimodal optical pulses composed of possibly many modes, the simplified modeling approach given by Eqs. (8) considers only two subpulses. Meanwhile, an extension of the above approach to pulse compounds with three and more subpulses has been accomplished [31,53].

Given the ansatz for two-color pulse compounds in the form of Eq. (7), initial conditions $A_0(t) \equiv A(z=0,t)$ that specify nonlinear photonic meta-atoms and two-color soliton molecules in terms of the subpulses A_1 and A_2 are different in some respects and are discussed separately in Section 3, and Section 4. Subsequently, we demonstrate the self-consistent z-propagation dynamics of these pulse compound, originally reported in Refs. [24,26,30,54,55], as well as their breakup in response to sufficiently large GV mismatches between both subpulses, originally reported in Ref. [25], in terms of numerical simulations governed by the full model Eq. (1). These numerical results demonstrate several theoretical findings reported by Hasegawa [1], applied to the concept of two-color pulse compounds.

In passing, let us stress that coupled equations of the form of Eqs. (8) comprise a much-used theoretical instrument for studying mutually bound solitons [3,56–62].

3. Nonlinear-photonics meta-atoms

Description of stationary trapped states. Subsequently we look for stationary solutions in the form of Eq. (7) under the additional constraint $\max(|A_2|) \ll \max(|A_1|)$. This allow to decouple Eqs. (8) and enables direct optical analogues of quantum mechanical bound-states [24,54,63]. Therefore, we assume the resulting two-color pulse compounds to consist of a strong trapping pulse, given by a solitary wave (S) at detuning $\Omega_S \equiv \Omega_1$, and a weak trapped pulse (TR) at detuning $\Omega_{TR} \equiv \Omega_2$. For the solitary wave part of the total pulse we neglect the XPM contribution in the nonlinear part of Eq. (8a) and assume

$$A_1(z,t) = U_S(t)\, e^{i\kappa' z}, \quad \text{with} \quad U_S(t) = \sqrt{P_0}\,\mathrm{sech}\left(\frac{t}{t_0}\right), \tag{9}$$

wherein $P_0 = |\beta_2'|/(\gamma' t_0^2)$, and $\kappa' = \beta_0 + \gamma' P_0/2$. Neglecting the SPM contribution in the nonlinear part of Eq. (8b) and making the ansatz

$$A_2(z,t) = \phi(t)\, e^{i\kappa'' z}, \tag{10}$$

the envelope $\phi(t)$ of a weak stationary trapped state is determined by the Schrödinger type eigenvalue problem

$$\left(-\frac{|\beta_2''|}{2}\frac{\mathrm{d}^2}{\mathrm{d}t^2} + V_S(t)\right)\phi_n(t) = \kappa_n\,\phi_n(t). \tag{11}$$

Therein, the solitary wave enters as a stationary attractive potential well $V_S(t) = -2\gamma'' P_0\,\mathrm{sech}^2(t/t_0)$. Hence, as pointed out above and discussed in the context of multimode optical pulses in glass fibers in Ref. [1], a weak pulse can be attracted by the intensity of the entire pulse if it exists in a domain of anomalous dispersion. Due to $\beta_2'' < 0$, this condition is met in the considered case. In analogy to the sech^2-potential in one-dimensional quantum scattering theory we may equivalently write the solitary-wave induced potential as [63]

$$V_S(t) = -\nu(\nu+1)\frac{|\beta_2''|}{2t_0^2}\,\mathrm{sech}^2\left(\frac{t}{t_0}\right), \quad \text{with} \quad \nu = -\frac{1}{2} + \left(\frac{1}{4} + 4\left|\frac{\gamma''}{\gamma'}\frac{\beta_2'}{\beta_2''}\right|\right)^{1/2}. \tag{12}$$

Moreover, due to the particular shape of the trapping potential, the eigenvalue problem Eq. (11) can even be solved exactly [63,64]. The number of trapped states of the potential in Eq. (12) is given by $N_{TR} = \lfloor \nu \rfloor + 1$, where $\lfloor \nu \rfloor$ is the integer part of the strength-parameter ν. From the analogy to the quantum mechanical scattering problem [64], the real-valued wavenumber eigenvalues can directly be stated as

$$\kappa_n = -\frac{|\beta_2''|}{2t_0^2}(\nu - n)^2, \quad \text{for} \quad n = 0, \ldots, \lfloor \nu \rfloor. \tag{13}$$

For a given value of n, they are related to Eq. (10) through $\kappa'' = \beta_0 - \kappa_n$. To each eigenvalue corresponds an eigenfunction ϕ_n with n zeros, specifying the $(n+1)$th fundamental solution of the eigenvalue problem Eq. (11). These solutions constitute the weak trapped states of the potential V_S. Referring to the Gaussian hypergeometric function as ${}_2F_1$ [65], and abbreviating $a_n = \frac{1}{2}(1+n)$ and $b_n = \frac{1}{2}(2\nu+1-n)$, they can be stated in closed form as [64]

$$\phi_n(t) = \begin{cases} \cosh^{\nu+1}\left(\frac{t}{t_0}\right)\ {}_2F_1\left[a_n, b_n; \frac{1}{2}; -\sinh^2\left(\frac{t}{t_0}\right)\right], & \text{for even } n, \\ \cosh^{\nu+1}\left(\frac{t}{t_0}\right)\ \sinh\left(\frac{t}{t_0}\right)\ {}_2F_1\left[a_n+\frac{1}{2}, b_n+\frac{1}{2}; \frac{3}{2}; -\sinh^2\left(\frac{t}{t_0}\right)\right], & \text{for odd } n. \end{cases} \tag{14}$$

Let us note that, as evident from the potential strength parameter ν in Eq. (12), the number N_{TR} of trapped states is uniquely defined by the four parameters β_2', β_2'', γ', and γ''. It is not affected by the duration t_0 of the trapping potential, which, according to Eq. (13), codetermines the value of the wavenumber eigenvalue of a fundamental solution.

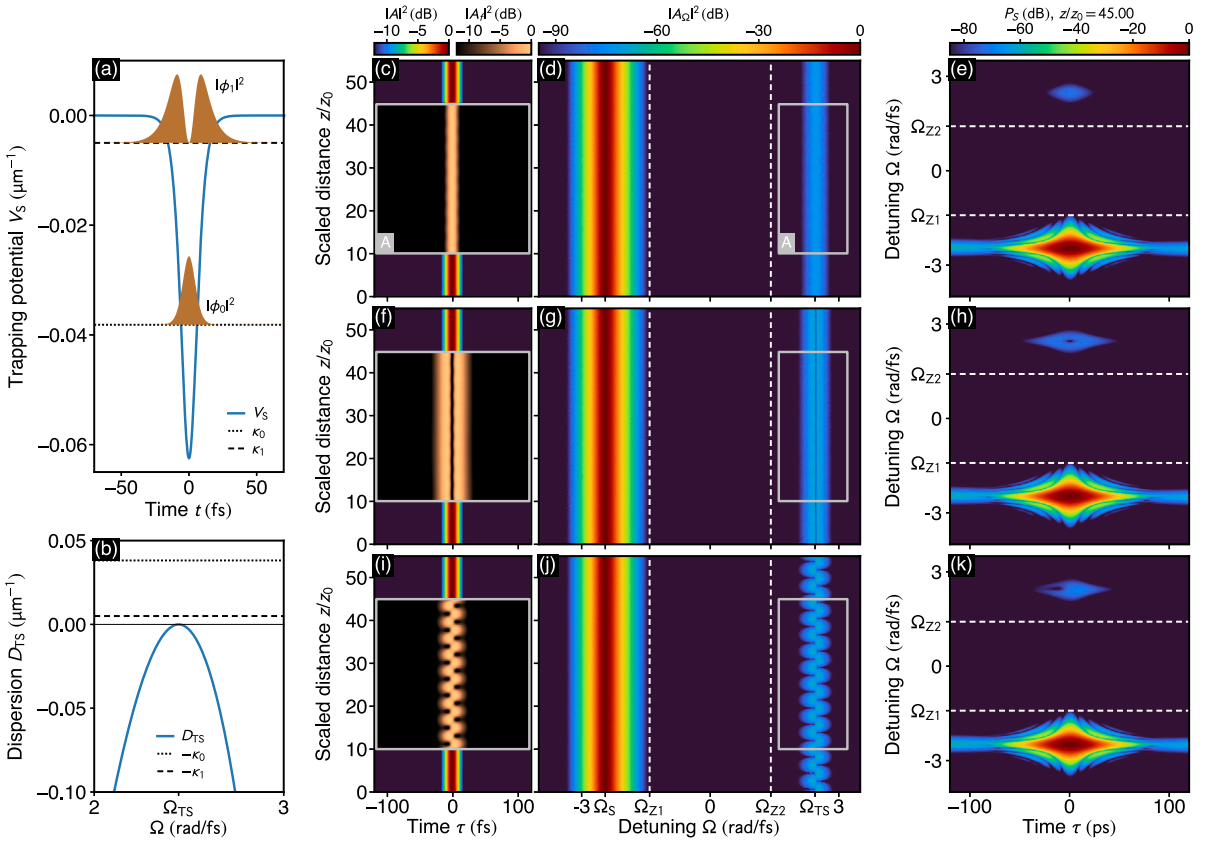

Fig. 2. Solitary-wave induced potential well exhibiting two trapped states. (a) Trapping potential V_S, wavenumber eigenvalues κ_n, and squared magnitude $|\phi_n|^2$ of trapped state eigenfunctions for $n = 0, 1$. (b) Dispersion profile $D_{TS}(\Omega)$ in the vicinity of the trapped state center frequency Ω_{TS}, (c) Time-domain propagation dynamics of the soliton and its lowest lying trapped state for $n = 0$. The propagation distance is scaled by the soliton period $z_0 = (\pi/2)(t_0^2/\beta_2') \approx 50$ μm. (d) Corresponding spectrum. The inverse Fourier transform of the part of the spectrum enclosed by the box (labeled A) in (d) is shown in the box (labeled A) in (c), providing a filtered view of the trapped state while leaving out the soliton part of the total pulse. (e) Spectrogram of the total pulse at $z/z_0 = 45$ for $\sigma = 8$ fs. (f,g,h) Same as (c,d,e) for the trapped state with $n = 1$. (i,j,k) Same as (c,d,e) for a superposition of both trapped states. Movies of the propagation dynamics are provided as supplementary material under Ref. [66].

Analogy to quantum mechanics. The eigenvalue problem Eq. (11) suggests an analogy to quantum mechanics, wherein a fundamental solution ϕ_n represents the wavefunction of a fictitious particle of mass $m = |\beta_2''|^{-1}$, confined to a localized, sech^2-shaped trapping potential V_S. The discrete variable $n = 0, \ldots, \lfloor \nu \rfloor$ resembles a principal quantum number that labels solutions with distinct wavenumbers, and the number of trapped state N_{TR} is similar to an atomic number. Consequently, a bare soliton, with none of its trapped states occupied, resembles the nucleus of an one-dimensional atom. By this analogy, a soliton along with its trapped states represents a nonlinear-photonics meta-atom.

3.1. Stable propagation of trapped states

Subsequently, we discuss the propagation dynamics of a nonlinear-photonics meta-atom with the ability to host two trapped states. More precisely, we consider an example for $\Omega_S = -2.828\,\mathrm{rad/fs}$ and $t_0 = 8\,\mathrm{fs}$, with $\Omega_{TR} = 2.828\,\mathrm{rad/fs}$ and $\nu \approx 1.566$. The resulting trapping potential and both its trapped states are shown in Fig. 2(a). In this case, the wavenumber eigenvalues are $(\kappa_0, \kappa_1) = (-0.0382, -0.0050)\,\mu\mathrm{m}^{-1}$, and the corresponding fundamental solutions take the simple form

$$\phi_0(t) = \mathrm{sech}^{\nu}\left(\frac{t}{t_0}\right), \quad \text{and,} \tag{15a}$$

$$\phi_1(t) = \mathrm{sech}^{\nu-1}\left(\frac{t}{t_0}\right)\tanh\left(\frac{t}{t_0}\right). \tag{15b}$$

As evident in Fig. 2(b), in the vicinity of Ω_{TR} and due to $\kappa'' > 0$ [Eq. (10)], a finite wavenumber-gap separates each trapped state from linear waves bound to the dispersion curve $D_{TR}(\Omega) \equiv \beta(\Omega) - \beta(\Omega_{TR}) - \beta_1(\Omega_{TR})(\Omega - \Omega_{TR}) < 0$. Therefore, we expect that trapped states composed by Eqs. (15) propagate in a stable manner. For the lowest lying trapped state, having order $n = 0$, this is demonstrated in

Figs. 2(c,d). These figures summarize pulse propagation simulations in terms of the modified NSE (1), using an initial condition of the form of Eq. (7) with A_1 as in Eq. (9), and A_2 as in Eq. (10) with $\phi(t) = \sqrt{10^{-7} P_0}\, \phi_0(t)$. In the time-domain propagation dynamics, shown in Fig. 2(c), a small drift of the soliton, caused by higher orders of dispersion at Ω_S [see Fig. 1], is accounted for by shifting to a moving frame of reference with time coordinate $\tau = t - \tilde{\beta}_1 z$ and $\tilde{\beta}_1 = 0.00637$ fs/μm. In Fig. 2(d), the vast frequency gap between the soliton and the trapped state is clearly visible. By means of an inverse Fourier transform of the frequency components belonging to the trapped state [box labeled A in Fig. 2(d)], an unhindered "filtered view" of the time-domain propagation dynamics of the trapped state is possible [box labeled A in Fig. 2(c)]. A spectrogram, providing a time–frequency view of the field at $z/z_0 = 45$, is shown in Fig. 2(d). The stable propagation of a trapped state with $n = 1$ for $\phi(t) = \sqrt{10^{-7} P_0}\, \phi_1(t)$, is detailed in Figs. 2(f–h). Finally, the simultaneous propagation of a superposition of both trapped states in the form $\phi(t) = \sqrt{10^{-7} P_0}\, [\phi_0(t) + 5\phi_1(t)]$ is shown in Figs. 2(i–k). The z-periodicity of the beating pattern visible in the time-domain propagation dynamics in Fig. 2(i), is a result of the different wavenumber eigenvalues of the trapped states, and is determined by $z_p = 2\pi/|\kappa_1 - \kappa_0| \approx 189$ μm ($z_p/z_0 \approx 3.8$). Thus, the coherent superposition of trapped states exhibits Rabi-type oscillations, similar to bound state dependent revival times in the quantum recurrence of wave packets [67,68].

Let us note that, bearing in mind that the number of bound states N_{TR} is determined by the potential strength parameter ν in Eq. (12), a setup with a different number of bound states can be obtained as well. This is possible by fixing Ω_S at some other feasible value, resulting in a different group-velocity matched detuning Ω_{TR}, implying different values of the parameters β_2', β_2'', γ', and γ''. For example, keeping $t_0 = 8$ fs but choosing $\Omega_S = -2.75$ rad/fs yields $\nu \approx 3.1$, resulting in a potential well with the ability to host $N_{TR} = 4$ trapped states. In such a case, however, phase-matched transfer of energy from the trapped states to dispersive waves within the domain of normal dispersion can be efficient [69].

3.2. Trapping-to-escape transition caused by a group-velocity mismatch

In the context of multimodal pulses in glass fibers in Ref. [1], the attraction of a wave packet by a potential well, created by the total pulse, was illustrated in terms of the kinetic equations of a fictitious particle associated with the wave packet. From a classical mechanics point of view, in order to ensure trapping of the wave packet by the total pulse, the velocity mismatch between the particle and the potential needs to be smaller than the escape velocity of the potential. Based on this view, and for a given velocity mismatch, the critical value of the total pulse intensity, required to achieve self-confinement, was determined [1]. In the presented work, pulse propagation simulations, such as those reported in Fig. 2, comprise a complementary approach to study the considered XPM induced attraction effect. Specifically, by keeping the detuning of the soliton fixed at $\Omega_S = \Omega_1$, but shifting the detuning of the trapped pulse to $\Omega_{TR} = \Omega_2 + \Delta\Omega$, we can enforce a group-velocity mismatch between both pulses and probe the stability of the meta-atom. For $\Delta\Omega > 0$ it is $\beta_1(\Omega_S) > \beta_1(\Omega_{TR})$, see Fig. 1(b). Thus, in a reference frame in which the soliton is stationary, the trapped state will initially have the propensity to move towards smaller times. This is demonstrated in Figs. 3(a,b) for the center frequency shift $\Delta\Omega = 0.05$ rad/fs. To assess the fraction of energy of the trapped state that is retained within the soliton induced potential well, we consider the quantity

$$e_{TR}(z) \equiv \frac{E_{TR}(z)}{E_{TR}(0)}, \quad \text{with} \quad E_{TR}(z) = \int_{-10\,t_0}^{10\,t_0} |\phi(z,\tau)|^2 \, \mathrm{d}\tau. \tag{16}$$

As evident from Fig. 3(e), at $\Delta\Omega = 0.05$ rad/fs, the trapped state is kept almost entirely within the well, i.e. $e_{TR} \approx 1$. In contrast, at $\Delta\Omega = 0.25$ rad/fs, a major share of the trapped pulse escapes the well during the initial propagation stage [Figs. 1(c,d)], indicated by the small value $e_{TR} \approx 0.3$ [Fig. 3(e)]. Let us note that, when viewing the considered pulse compounds as meta-atoms, the quantity $1 - e_{TR}(z)$ specifies the fraction of trapped energy that is radiated away, resembling an ionization probability for quantum mechanical atoms. A parameter study, detailing the dependence of e_{TR} as function of the center frequency shift $\Delta\Omega$ is summarized in Fig. 3(f). The transition from trapping to escape can be supplemented by an entirely classical picture similar as in Ref. [1]: from a classical point of view we might expect that a particle, initially located at the center of the well, remains confined to the well if its "classical" kinetic energy $T_{kin} = \frac{1}{2} m \Delta\beta_1^2 = \frac{1}{2} |\beta_2''|^{-1} \left[\beta_1(\Omega_S) - \beta_1(\Omega_{TR})\right]^2$ does not exceed the well depth $V_0 = 2\gamma'' P_0$. As evident from Fig. 3, the findings based on this classical picture complement the results obtained in terms of direct simulations of the modified NSE (1) very well. The above results clearly demonstrate the limits of stability of nonlinear photonics meta-atoms with respect to a group-velocity mismatch between the trapping soliton and the trapped state. These findings are consistent with our previous results on the break-up dynamics of two-color pulse compounds [25].

4. Two-color soliton molecules

Seeding of tightly bound two-color pulse compounds. When considering initial conditions of the form of Eq. (7), with A_1 a fundamental nonlinear Schrödinger soliton as in Eq. (9), and A_2 a trapped state as in Eq. (10) with $\phi(t) = r\sqrt{P_0}\, \phi_0(t)$, the XPM contribution of the weak trapped pulse onto the trapping soliton can be heightened by increasing the parameter r. This is demonstrated in Figs. 4(a–c), where pulse propagation simulations in terms of the modified NSE (1) are shown for different values of r, significantly larger than those considered in the preceding section. Especially for larger values of r [Figs. 4(b,c)], the intensity exhibits the following dynamics: the mutual confining action of XPM results in a contraction of both subpulses, prompting the formation of a narrow localized pulse compound. A similar effect has previously been suggested by Hasegawa for multimode optical pulses in glass fibers in Ref. [1], where he writes "[...] as many modes are trapped, the peak intensity of the packet increases quite analogously to a gravitational instability, resulting in a further contraction of the packet." (Ref. [1], p. 417). The results shown in Figs. 4(a–c)

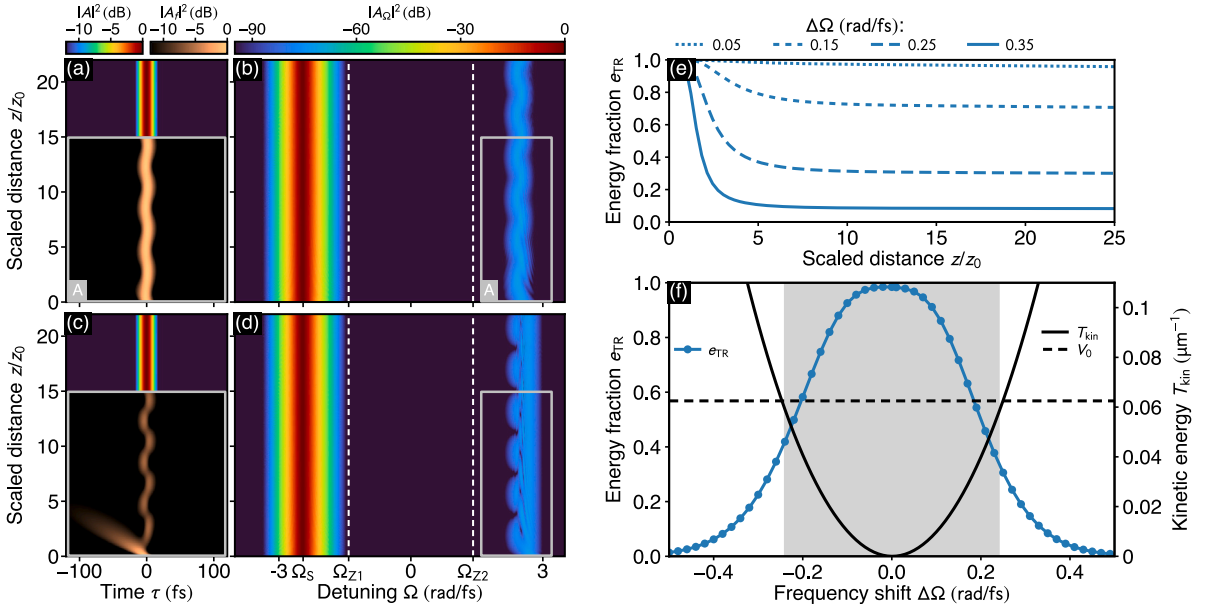

Fig. 3. Characterization of the transition from trapping to escape. (a) Time-domain propagation dynamics of the soliton and its lowest lying trapped state ($n = 0$) shifted from Ω_{TS} to $\Omega_{\mathrm{TS}} + \Delta\Omega$ for $\Delta\Omega = 0.05$ (rad/fs). (b) Corresponding spectrum. The inverse Fourier transform of the part of the spectrum enclosed by the box (labeled A) in (b) is shown in the box (labeled A) in (a). This provides a filtered view of the trapped state with the benefit of leaving out the soliton part of the total pulse. (c,d) Same as (a,b) for $\Delta\Omega = 0.25$ (rad/fs). (e) Fraction of trapped energy as function of the propagation distance. (f) Fraction of trapped energy as function of the trapped state center frequency shift. Secondary ordinate shows the potential depth (V_0) as well as the kinetic energy T_{kin} of the fictitious classical particle. Parameter range in which the particle cannot escape the well is shaded gray. Movies of the propagation dynamics shown in (a–d) are provided as supplementary material under Ref. [66].

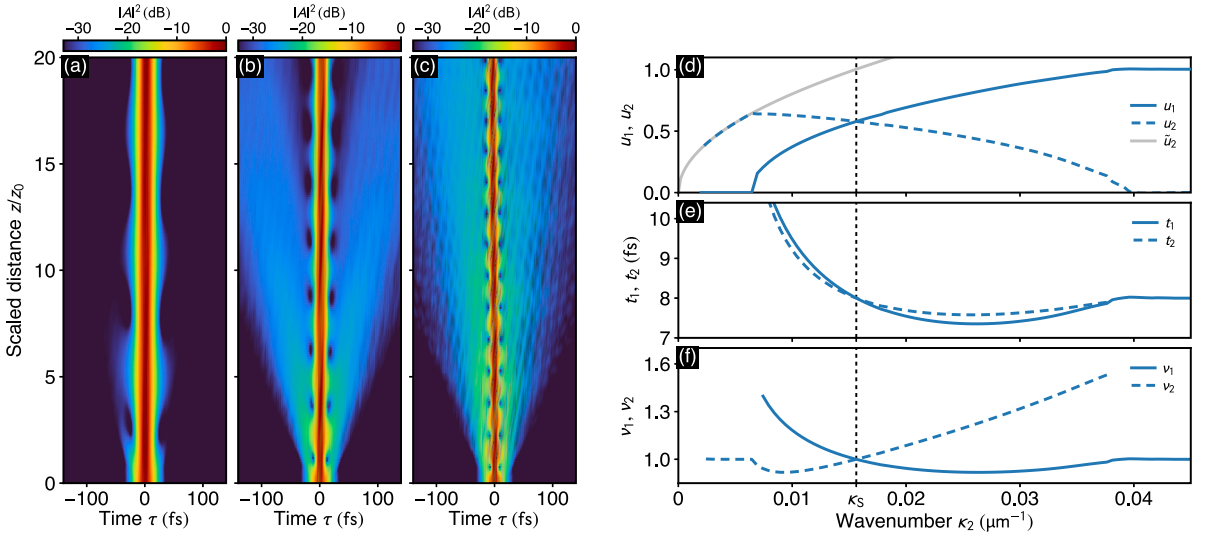

Fig. 4. Transition from trapping to tightly bound, molecule-like two-color pulse compounds. (a) Time-domain propagation dynamics arising from an initial condition with $\phi(t) = \sqrt{0.1 P_0}\,\phi_0(t)$ (see text). (b) Same as (a) for $\phi(t) = \sqrt{0.5 P_0}\,\phi_0(t)$. (c) Same as (a) for $\phi(t) = \sqrt{P_0}\,\phi_0(t)$. (d-f) Solutions of the coupled ODEs (18), fitted to functions of the form $U_m = U_{0,m}\mathrm{sech}^{\nu_m}(t/t_m)$, for $m = 1, 2$. (d) Scaled pulse amplitudes $u_n = U_{0,m}/\sqrt{P_0}$, (e) pulse durations t_n, and, (f) pulse shape exponents ν_m, $m = 1, 2$. In (d), $\tilde{u}_2$ indicates the peak amplitude of a fundamental NSE soliton with wavenumber κ_2. Vertical dashed lines in (d-f) mark $\kappa_{\mathrm{S}} = 0.0156$ μm^{-1}.

demonstrate this effect in the context of two-color pulse compounds in nonlinear fibers or waveguides with two zero-dispersion points. Let us note that, for $r \approx 1$, initial conditions as pointed out above directly generate tightly bound, mutually confined two-color pulse compounds. They are accompanied by radiation, emanating from the localized state upon propagation, and can exhibit internal dynamics reminiscent molecular vibrations [24,25,31,70]. However, such a seeding procedure generates two-color pulse compounds in a largely uncontrolled manner.

Simultaneous solutions of the coupled equations. We can surpass the above seeding approach by directly searching for simultaneous solitary-wave solutions of the coupled nonlinear Eqs. (8) beyond the linear limit discussed in Section 3. Substituting an ansatz for two subpulses, labeled $m = 1, 2$, in the form of

$$A_m(z,t) = U_m(t)\, e^{i(\beta_0+\kappa_m)z}, \quad \text{with} \quad m = 1,2 \tag{17}$$

into Eqs. (8), yields two coupled ordinary differential equations (ODEs) of second order

$$\ddot{U}_1 - \frac{2}{\beta_2'}\left[\gamma'\left(|U_1|^2 + 2|U_2|^2\right) - \kappa_1\right] U_1 = 0, \tag{18a}$$

$$\ddot{U}_2 - \frac{2}{\beta_2''}\left[\gamma''\left(|U_2|^2 + 2|U_1|^2\right) - \kappa_2\right] U_2 = 0, \tag{18b}$$

for two real-valued envelopes $U_m \equiv U_m(t)$, $m = 1, 2$, with dots denoting derivatives with respect to time. Under suitable conditions, solitary-wave solutions for the coupled nonlinear Eqs. (18) can be specified analytically [30,60,71–73]. Approximate solutions based on parameterized trial functions can be found, e.g., in terms of a variational approach [74]. In order to obtain simultaneous solutions $U_1(t)$, and $U_2(t)$ under more general conditions, Eqs. (18) need to be solved numerically. This can be achieved, e.g., by spectral renormalization methods [75–78], shooting methods [8,9], squared operator methods [79], conjugate gradient methods [80,81], z-propagation adapted imaginary-time evolution methods [82,83], or Newton-type methods [84]. Here, in order to solve for simultaneous solutions of the ODEs (18), we employ a Newton method that is based on a boundary value Runge–Kutta algorithm [85]. So as to systematically obtain solutions $U_1(t)$ and $U_2(t)$, we keep five of the six parameters that enter Eqs. (18) fixed. Therefore we set β_2', β_2'', γ', and γ'' to the values considered throughout the preceding section, and preset the wavenumber $\kappa_1 = |\beta_2'|(2t_0^2)^{-1} \approx 0.0156\ \mu\text{m}^{-1}$ of a fundamental nonlinear Schrödinger soliton with $t_0 = 8\,\text{fs}$ in Eq. (18a). We then sweep the remaining parameter κ_2 over the wavenumber range $(0.002, 0.05)\ \mu\text{m}^{-1}$, enclosing the value of κ_1. We start the parameter sweep at $\kappa_2 = 0.05\ \mu\text{m}^{-1}$, which vastly exceeds the wavenumber eigenvalue of the lowest lying trapped state solution at $0.0382\ \mu\text{m}^{-1}$. Above this value, we expect U_2 to vanish, and U_1 to yield a fundamental soliton $U_1(t) = \sqrt{P_0}\,\text{sech}(t/t_0)$ with $P_0 = |\beta_2'|(\gamma' t_0^2)^{-1}$. We set initial trial functions for U_1 and U_2 with parity similar to the soliton and the lowest lying trapped state, and continue the obtained solutions to smaller values of κ_2. The results of this parameter sweep are summarized in Figs. 4(d–f). We find that all solutions can be parameterized in the form $U_m(t) = U_{0,m}\,\text{sech}^{\nu_m}(t/t_m)$, with pulse peak amplitudes $U_{0,m}$ [Fig. 4(d)], pulse durations t_m [Fig. 4(e)], and pulse shape exponents ν_m [Fig. 4(f)], for $m = 1, 2$. In agreement with the results reported in Section 3.1, we find that a weak nonzero solution U_2 with $t_2 = 8$ fs and $\nu_2 \approx 1.55$ originates at $\kappa_2 \approx 0.038\ \mu\text{m}^{-1}$. For $\kappa_2 < 0.038\ \mu\text{m}^{-1}$, the peak amplitude of the subpulse $m = 1$ continuously decreases while that for $m = 2$ increases. Below $\kappa_2 \approx 0.007\ \mu\text{m}^{-1}$, subpulse U_1 vanishes and U_2 describes a fundamental soliton with pulse shape parameter $\nu_2 = 1$ and wavenumber κ_2. To facilitate intuition, we included the amplitude of a free soliton with wavenumber κ_2, i.e. peak amplitude $\tilde{U}_{0,2} = \sqrt{2\kappa_2/\gamma''}$, in Fig. 4(d). Let us note that the intermediate parameter range $0.007\ \mu\text{m}^{-1} < \kappa_2 < 0.038\ \mu\text{m}^{-1}$ bears tightly coupled pulse compounds, characterized by subpulse amplitudes with similar peak heights, see Fig. 4(d).

4.1. Two-color soliton pairs

Upon closely assessing the results shown in Figs. 4(d–f), we find that at $\kappa_2 = 0.0156\ \mu\text{m}^{-1}$, a pair of matching solutions with plain hyperbolic-secant shape $U_m(t) = U_{0,m}\,\text{sech}(t/t_0)$, $m = 1, 2$, is attained. This can be traced back to the uniformity of Eqs. (18a) and (18b) for the considered set of parameters. Formally, by assuming $\kappa \equiv \kappa_1 = \kappa_2$ and $U \equiv U_1 = U_2$, both equations take the form of a standard NSE with modified parameters

$$-\frac{\beta_2'}{2}\frac{\mathrm{d}^2}{\mathrm{d}t^2}U(t) + 3\gamma'|U(t)|^2U(t) = \kappa U(t), \tag{19}$$

where, for convenience only, we used the parameters of Eq. (18a). The real-valued pulse envelope U should therefore be identified by the peak intensity $\tilde{P}_0 = |\beta_2'|(3\gamma' t_0^2)^{-1}$, and thus $u_1 = u_2 = \sqrt{1/3} \approx 0.57$ in Fig. 4(d). Hence, at $\kappa_2 = 0.0156\ \mu\text{m}^{-1}$, both subpulses resemble true two-color *soliton* pairs: the pulse envelopes U_1 and U_2 both specify a fundamental NSE soliton; for each pulse, its binding partner modifies the nonlinear coefficient of the underlying NSE through XPM, helping the pulse sustain its shape. Consequently, both pulses can only persist conjointly as a bonding unit. This special case is consistent with a description of two-color pulse compounds in terms of incoherently coupled pulses [30]. By considering the ansatz Eq. (7), we can plug in the obtained pulse envelopes for U_1 and U_2 and resubstitute the parameters that define the propagation constant in Section 2 to obtain

$$A(z,t) = F(z,t)\,\cos\left(\sqrt{\frac{6\beta_2}{|\beta_4|}}\,t\right) e^{-i\beta_0 z}, \quad \text{with} \quad F(z,t) = \sqrt{\frac{8\beta_2}{3\gamma t_0^2}}\,\text{sech}\left(\frac{t}{t_0}\right) e^{i\kappa z}, \quad \text{and} \quad \kappa = \frac{\beta_2}{t_0^2}. \tag{20}$$

Let us note that F is equivalent to the fundamental meta-soliton obtained in Ref. [26], which becomes evident when substituting $\epsilon = t_0^{-1}[3\beta_2/(2|\beta_4|)]^{-1/2}$ and $\mu_0\epsilon^2 = \beta_2/t_0^2$. This fundamental meta-soliton was first formulated by Tam et al., when studying stationary solutions for the modified NSE (1) by putting emphasis on the time-domain representation of the field in terms of a multi-scales analysis [26]. This unveiled a large superfamily of solitons, now referred to as generalized dispersion Kerr solitons. We would like to point out that within the presented approach, i.e. by putting emphasis on the frequency-domain representation of two-color pulse compounds, the fundamental meta-soliton is derived with great ease. Furthermore, both approaches complement each other very

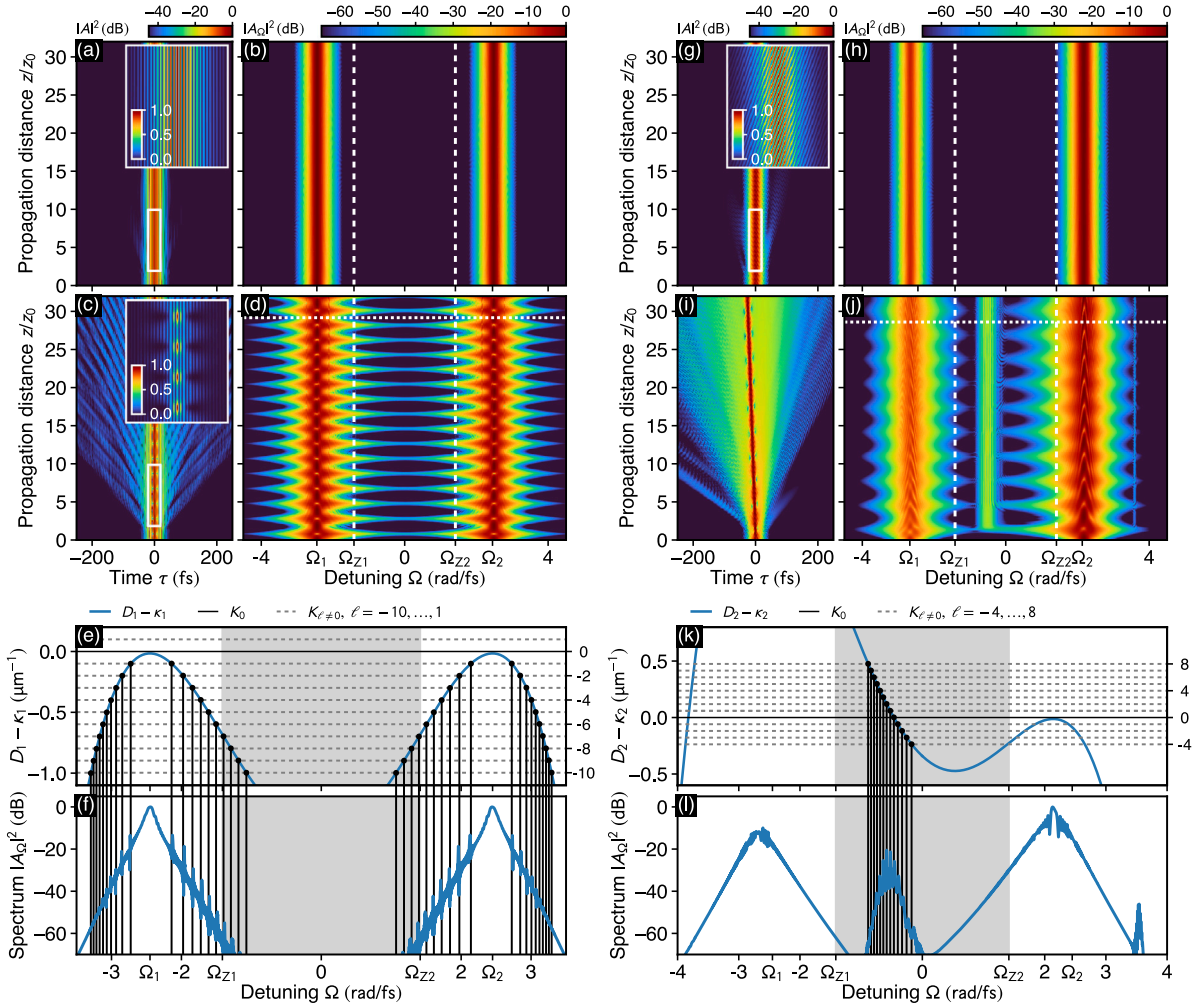

Fig. 5. Resonant radiation of two-color soliton molecules. (a,b) Stationary propagation of a soliton molecule with subpulse loci at $\Omega_1 = -\Omega_2 = 2.828$ rad/fs. (a) Time-domain propagation dynamics. The inset shows a close-up view of $|A(z,\tau)|^2/\max(|A(0,\tau)|^2)$ in the range $\tau = -20 \ldots 20$ fs and $z/z_0 = 2 \ldots 10$. (b) Corresponding spectrum. (c,d) Same as (a,b) for soliton molecule order $N = 1.8$. Horizontal dashed line in (d) indicates $z/z_0 = 29.2$. (e) Dispersion profile and graphical solution of the resonance conditions Eqs. (22) for z-oscillation periods of order $m = -10 \ldots 1$. (f) Spectrum at $z/z_0 = 29.2$. (g–l) Same as (a–f) for a soliton molecule with subpulse loci at $\Omega_1 = -2.674$ rad/fs and $\Omega_2 = 2.134$ rad/fs. In (i,j) the soliton molecule order is $N = 1.6$. Horizontal dashed line in (j) indicates $z/z_0 = 28.6$. The time-domain propagation dynamics is shown in a moving frame of reference where $\tau = t - \tilde{\beta}_1 z$. In (a), (c) $\tilde{\beta}_1 = 0$ fs/μm. In (g), (i) $\tilde{\beta}_1 = 0.509$ rad/fs. Propagation distance is scaled by $z_0 = 32$ μm. Movies of the propagation dynamics shown in (a–d) and (g–j) are provided as supplementary material under Ref. [66].

well. Further, the above two-color soliton pairs resemble vector solitons studied in the context of birefringent optical fibers [61,86–90]. The stationary propagation of the two-color soliton pair defined by Eq. (20) in terms of the modified NSE (1) is demonstrated in Figs. 5(a,b). The inset in Fig. 5(a) provides a close-up view onto the localized pulse, indicating interference fringes with period $\Delta t \approx \sqrt{|\beta_4|/(6\beta_2\pi^2)} \approx 1.3$ fs that are due to the cosine in Eq. (20). These interference fringes appear stationary since the propagation scenario exhibits the symmetry $\beta(\Omega_1) = \beta(\Omega_2)$ and $\kappa_1 = \kappa_2$. A spectrogram of the propagation scenario at $z/z_0 = 29.17$ is shown in Fig. 6(a). A small amount of residual radiation can be seen to lie right on the curve $\beta_1(\Omega)z$, given by the short-dashed line in Fig. 6(a). It was emitted by the pulse compound during the initial propagation stage and is caused by the presence of higher orders of dispersion at the individual subpulse loci, which were neglected in the simplified description leading to Eqs. (20).

4.2. Kushi-comb-like multi-frequency radiation

Previously, it was shown that z-periodic amplitude and width oscillations of two-color soliton molecules can be excited in a systematic manner by increasing their initial peak amplitude by some factor N according to $F(z,t) \leftarrow NF(z,t)$ [26,55]. In analogy to usual nonlinear Schrödinger solitons, values $N > 1$ define higher order metasolitons. Recently, we have performed a comprehensive analysis of the amplitude oscillations of such higher order metasolitons, indicating that with increasing N, the number of spatial

Fourier-modes needed to characterize their peak-intensity variation, increases [55]. In other words, with increasing strength of perturbation of a soliton molecule, its dynamics changes from harmonic to nonlinear oscillations.

Degenerate multi-frequency radiation. To demonstrate amplitude and width oscillations, we show the propagation dynamics of a symmetric soliton molecule of order $N = 1.8$, based on the two-color soliton pair (20), in Figs. 5(c,d). As can be seen from the time-domain dynamics in Fig. 5(c), the localized pulse exhibits periodic amplitude and width variations [close-up view in Fig. 5(c)], and emits radiation along either direction along the coordinate t in a symmetric fashion. Quite similar dynamics where obtained using the seeding approach in Figs. 4(b,c). The oscillation of the soliton molecule is also clearly visible in the spectrum shown in Fig. 5(d). As evident from Fig. 5(f), at $z/z_0 \approx 29.17$ it exhibits comb-like bands of frequencies in the vicinity of the subpulse loci Ω_1 and Ω_2. The location of these newly generated frequencies can be understood by extending existing approaches for the derivation of resonance conditions [91–95] to two-color pulse compounds [55,70]. Below, we summarize these resonance conditions, which where obtained by assuming a dynamically evolving pulse compound of the form [70]

$$U_m(z,t) = \sum_{\ell} C_{m\ell}(t)\, \exp\left[i\left(\kappa_m + K_\ell\right) z\right], \quad \text{with} \quad m \in (1,2),\ \ell \in \mathbb{Z}. \tag{21}$$

In Eq. (21), $C_{m\ell}$ are expansions coefficients, and κ_m indicate wavenumbers that govern the z-propagation of each subpulse. The wavenumbers of the higher harmonics of the z-oscillation period are $K_\ell = 2\pi\ell/\Lambda$, with Λ referring to the z-oscillation wavelength of the pulse compound and ℓ labeling the corresponding order. Based on this ansatz, the resonance conditions

$$D_m(\Omega_{RR}) - \kappa_m = K_\ell, \quad \text{with} \quad m \in (1,2),\ \ell \in \mathbb{Z}, \quad \text{and} \tag{22a}$$

$$D_m(\Omega_{RR}) - 2\kappa_m + \kappa_{m'} = K_\ell, \quad \text{with} \quad m, m' \in (1,2),\ m \neq m',\ \ell \in \mathbb{Z}, \tag{22b}$$

with dispersion profiles $D_m(\Omega) \equiv \beta(\Omega) - \beta(\Omega_m) - \beta_1(\Omega)(\Omega - \Omega_m)$ for $m = 1, 2$, can be derived [70]. In Eqs. (22), Ω_{RR} specifies those frequencies at which resonant radiation (RR) is excited. While Eq. (22a) defines resonance conditions for the generation of Cherenkov radiation by each subpulse, Eq. (22b) defines additional resonance conditions indicative of four-wave mixing (FWM) processes involving both subpulses.

For the considered soliton molecule of order $N = 1.8$, we find $\Lambda \approx 63\ \mu\text{m} \approx 2z_0$ [with $z_0 = 32\ \mu\text{m}$, see Fig. 5(d)]. In this case, the aforementioned symmetry $\kappa_1 = \kappa_2$ renders Eqs. (22a) and (22b) degenerate. As evident from the graphical solution of Eqs. (22) in Fig. 5(e), the resonance conditions predict the newly generated frequencies in Fig. 5(f) very well. A spectrogram of the propagation scenario at $z/z_0 = 29.17$ is shown in Fig. 6(b). Therein, the multi-peaked spectral bands, at which the oscillating soliton molecule sheds radiation, are reminiscent of the shape of traditional Japanese Kushi combs.

Non-degenerate multi-frequency radiation. Let us note that, due to the wide variety of two-color pulse compounds with different substructure, their emission spectra manifest in various forms. For example, considering a pair of group-velocity matched detunings different from the one considered above, the degeneracy among Eqs. (22) can be lifted. Subsequently we take $\Omega_1 = -2.674\ \text{rad/fs}$ and $\Omega_2 = 2.134\ \text{rad/fs}$, for which $\beta_1' = 0.514\ \text{fs/}\mu\text{m}$, $\beta_1'' = 0.514\ \text{fs/}\mu\text{m}$, $\beta_2' = -2.576\ \text{fs}^2/\mu\text{m}$, and, $\beta_2'' = -1.278\ \text{fs}^2/\mu\text{m}$. In terms of the coupled ODEs (18) we then determine a pair of simultaneous solutions which specify the initial condition

$$A_0(t) = U_{0,1}\, \text{sech}^{\nu_1}\left(\frac{t}{t_1}\right) e^{-i\Omega_1 t} + U_{0,2}\, \text{sech}^{\nu_2}\left(\frac{t}{t_2}\right) e^{-i\Omega_2 t}, \tag{23}$$

with parameters $U_{0,1} = 0.050\ \sqrt{\text{W}}$, $U_{0,2} = 0.141\ \sqrt{\text{W}}$, $t_1 = 7.207\ \text{fs}$, $t_2 = 7.271\ \text{fs}$, $\nu_1 = 0.901$, and $\nu_2 = 1.022$. The stationary propagation of this soliton molecule with non-identical subpulses is shown in Fig. 4(g,h). As a consequence of the broken subpulse-symmetry, the interference fringes that characterize the pulse compound are not stationary any more [close-up view in Fig. 5(g)]. The fact that the pulse compound remains localized, despite its envelope exhibiting a non-stationary profile, might be the reason why no such objects could be found using a time-domain based Newton conjugate-gradient method [26]. Next, we increase the order of this soliton molecule to $N = 1.6$, resulting in the propagation dynamics with z-oscillation period $\Lambda \approx 106\ \mu\text{m} \approx 3.3z_0$ shown in Figs. 5(i,j). In this case, a pronounced multi-peaked spectral band of frequencies within the domain of normal dispersion is excited [see Figs. 5(j,l)]. These newly generated frequencies can be linked to multi-frequency Cherenkov radiation emitted by the subpulse at Ω_2, as can be seen from the graphical solution of the resonance conditions (22a), shown in Fig. 5(k). Let us note that similar coupling phenomena of localized states to the continuum have earlier been observed for solitons in periodic dispersion profiles [93], oscillating bound solitons in twin-core fibers [94], and dissipative solitons in nonlinear microring resonators [95]. A further band of frequencies, excited in the vicinity of $\Omega \approx 3.5\ \text{rad/fs}$ can be attributed to FWM-resonances described by Eq. (22b). A spectrogram of the propagation scenario at $z/z_0 = 28.6$ is shown in Fig. 6(c), unveiling that the resonant radiation emanates from the oscillating soliton molecule in a pulse-wise fashion.

5. Summary and conclusions

In summary, we have discussed several aspects of the z-propagation of two-color pulse compounds in a modified NSE with positive group-velocity dispersion coefficient and negative fourth-order dispersion coefficient. Therefore, we considered the interaction dynamics of two pulses in distinct domains of anomalous dispersion, group-velocity matched despite a large frequency gap.

We have demonstrated that their mutual confining action can manifest itself in different forms, depending on the relative strength of SPM and XPM felt by each pulse. In the limiting case where the resulting bound states consist of a strong trapping pulse, given

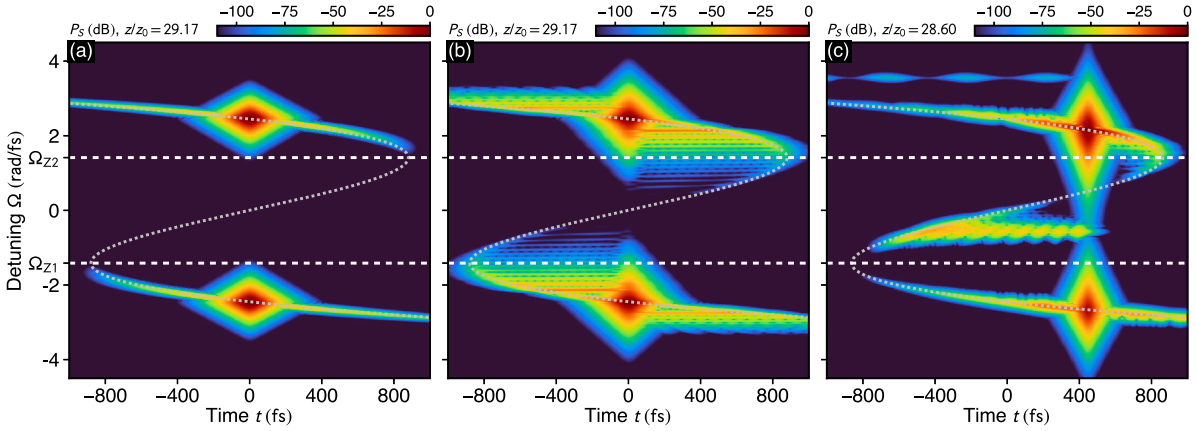

Fig. 6. Spectrograms of selected soliton molecules. (a) Two-color soliton pair of Figs. 5(a,b) at $z/z_0 = 29.17$, computed using $\sigma = 30$ fs in Eq. (6). (b) Oscillating, symmetric soliton molecule of Figs. 5(c,d) at $z/z_0 = 29.17$ for $\sigma = 30$ fs, showing many narrowly spaced resonances reminiscent of the shape of traditional Japanese Kushi combs. (c) Oscillating, non-symmetric soliton molecule of Figs. 5(i,j) at $z/z_0 = 28.6$ for $\sigma = 20$ fs. The pulse-wise emission of radiation, synchronized with the periodic amplitude and width variations of the pulse compound, is clearly visible. In (a-c), the short-dashed line shows $\beta_1(\Omega)\, z$, indicating the delimiting temporal position of a mode at detuning Ω, emitted at $z = 0$. Movies of the propagation dynamics are provided as supplementary material under Ref. [66].

by a soliton, and a weak trapped pulse, we have shown that optical analogues of quantum mechanical bound states can be realized that are determined by a Schrödinger-type eigenvalue problem [24]. The resulting photonic meta-atoms even support Rabi-type oscillations of its trapped states, similar to the recurrence dynamics of wave packets in quantum wells [67]. We further probed the limits of stability of these meta-atoms by imposing a group-velocity mismatch between the trapping soliton and the trapped pulse. With increasing strength of perturbation, parts of the trapped state escapes the soliton, similar in effect to the ionization of quantum mechanical atoms. These findings complement our earlier results on the break-up dynamics of two-color pulse compounds [95].

For the more general case where the mutual confining action between the pulses is dominated by XPM, we have discussed a simplified modeling approach, allowing to determine simultaneous solutions for the bound pair of pulses. The resulting solutions feature the above meta-atoms as limiting cases when the disparity of the subpulse amplitudes is large. Further, by exploiting symmetries of the underlying propagation model, a special class of solutions, forming true two-color soliton pairs [30], was characterized in closed form. This special class of solutions, referred to as generalized dispersion Kerr solitons, has also been derived in Ref. [26]. We have presented numerical results demonstrating the complex propagation dynamics of such pulse compounds, which we here referred to as two-color soliton molecules. Specifically, we have shown that soliton molecules exhibit highly robust vibrational characteristics, a behavior that is difficult to achieve in a conservative NSE system. These non-stationary, z-periodic dynamics of the subpulses triggers the emission of resonant radiation. The location of the resulting multi-peaked spectral bands can be precisely predicted by means of phase-matching conditions [55,70]. Due to the manifold of soliton molecules with different substructure, their emission spectra manifest in various complex forms. Most notably, if the oscillating soliton molecule consists of a pair of identical subpulses, inherent symmetries lead to degeneracies in the resonance spectrum, causing their spectrogram trace to resemble the shape of Japanese Kushi combs. Additional perturbations lift existing degeneracies and result in more complex emission spectra which are characterized by distinct spectral bands that can be separately linked to resonant Cherenkov radiation and additional four-wave mixing processes. The occurrence of such multi-frequency radiation, especially in the degenerate form, comprises a fundamental phenomenon in nonlinear waveguides with multiple zero-dispersion points and sheds light onto the puzzling propagation dynamics of two-frequency pulse compounds, resembling the generation of radiation by vibrating molecules.

Finally, let us note that we recently extended the range of systems in which such two-color pulse compounds are expected to exist. Therefore, we considered waveguides with a single zero-dispersion point and frequency dependent nonlinearity with a zero-nonlinearity point [96,97]. In such waveguides, soliton dynamics in a domain of normal dispersion can be achieved by a negative nonlinearity [98,99]. In the corresponding description of pulse compounds in terms of the simplified model (8), having $\beta_2' < 0$ and $\beta_2'' > 0$ then requires $\gamma' > 0$ and $\gamma'' < 0$, and the potential well in the eigenproblem corresponding to Eq. (11) is ensured by $\gamma'' < 0$ [54]. We studied the above binding mechanism for incoherently coupled two-color pulse compounds in such waveguides, demonstrating meta-atoms and molecule-like bound states of pulses that persist in the presence of the Raman effect [31,54], allowing to understand the complex propagation dynamics observed in a recent study on higher-order soliton evolution in a photonic crystal fiber with one zero-dispersion point and frequency dependent nonlinearity [100].

Declaration of competing interest

The authors declare that they have no known competing financial interests or personal relationships that could have appeared to influence the work reported in this paper.

Data availability

Data will be made available on request.

Acknowledgments

We acknowledge support from the Deutsche Forschungsgemeinschaft (DFG), Germany under Germany's Excellence Strategy within the Cluster of Excellence PhoenixD (Photonics, Optics, and Engineering – Innovation Across Disciplines) (EXC 2122, projectID 390833453). All authors approved the version of the manuscript to be published.

References

[1] A. Hasegawa, Self-confinement of multimode optical pulse in a glass fiber, Opt. Lett. 5 (1980) 416.
[2] V.V. Afanas'ev, E.M. Dianov, V.N. Prokhorov, A.M. Serkin, Nonlinear pairing of light and dark optical solitons, Pis'Ma Zh. Eksp. Teor. Fiz. 48 (1988) 588; JETP Lett. 48 (1988) 638.
[3] V.V. Afanasjev, E.M. Dianov, V.N. Serkin, Nonlinear pairing of short bright and dark soliton pulses by phase cross modulation, IEEE J. Quantum Electron. 25 (1989) 2656.
[4] C.R. Menyuk, Stability of solitons in birefringent optical fibers. I: Equal propagation amplitudes, Opt. Lett. 12 (1987) 614.
[5] F. Mitschke, Fiber Optics: Physics and Technology, Springer, 2016.
[6] G.P. Agrawal, Nonlinear Fiber Optics, Academic Press, 2019.
[7] P.G. Drazin, R.S. Johnson, Solitons: An Introduction, Cambridge University Press, 1989.
[8] M. Haelterman, A. Sheppard, Bifurcation phenomena and multiple soliton-bound states in isotropic Kerr media, Phys. Rev. E 149 (1994) 3376.
[9] M. Mitchell, M. Segev, T. Coskun, D. Christodulides, Theory of self-trapped spatially incoherent light beams, Phys. Rev. Lett. 79 (1997) 4990.
[10] B. Tan, J.P. Boyd, Coupled-mode envelope solitary waves in a pair of cubic Schrödinger equations with cross modulation: Analytical solution and collisions with application to Rossby waves, Chaos Solitons Fractals 11 (2000) 1113.
[11] B. Tan, S. Liu, Collision interactions of solitons in a Baroclinic atmosphere, J. Atmos. Sci. 52 (1995) 1501–1512.
[12] A. Demircan, S. Amiranashvili, G. Steinmeyer, Controlling light by light with an optical event horizon, Phys. Rev. Lett. 106 (2011) 163901.
[13] R. Smith, The reflection of short gravity waves on a non-uniform current, Math. Proc. Cambridge Philos. Soc. 78 (1975) 517.
[14] C.M. de Sterke, Optical push broom, Opt. Lett. 17 (1992) 914.
[15] T.G. Philbin, C. Kuklewicz, S. Robertson, S. Hill, F. König, U. Leonhardt, Fiber-optical analog of the event horizon, Science 319 (2008) 1367–1370.
[16] D. Faccio, Laser pulse analogues for gravity and analogue Hawking radiation, Cont. Phys. 53 (2) (2012) 97–112.
[17] B.W. Plansinis, W.R. Donaldson, G.P. Agrawal, What is the temporal analog of reflection and refraction of optical beams? Phys. Rev. Lett. 115 (2015) 183901.
[18] A. Demircan, S. Amiranashvili, C. Brée, G. Steinmeyer, Compressible Octave spanning supercontinuum generation by two-pulse collisions, Phys. Rev. Lett. 110 (2013) 233901.
[19] A. Demircan, S. Amiranashvili, C. Brée, U. Morgner, G. Steinmeyer, Adjustable pulse compression scheme for generation of few-cycle pulses in the midinfrared, Opt. Lett. 39 (2014) 2735.
[20] I. Babushkin, S. Amiranashvili, C. Brée, U. Morgner, G. Steinmeyer, A. Demircan, The effect of chirp on pulse compression at a group velocity horizon, IEEE Photonics J. 8 (2016) 1.
[21] R. Driben, F. Mitschke, N. Zhavoronkov, Cascaded interactions between Raman induced solitons and dispersive waves in photonic crystal fibers at the advanced stage of supercontinuum generation, Opt. Express 18 (25) (2010) 25993–25998.
[22] A. Demircan, S. Amiranashvili, C. Brée, C. Mahnke, F. Mitschke, G. Steinmeyer, Rogue wave formation by accelerated solitons at an optical event horizon, Appl. Phys. B 115 (2014) 343–354.
[23] D.V. Skryabin, A.V. Gorbach, Colloquium: Looking at a soliton through the prism of optical supercontinuum, Rev. Modern Phys. 82 (2010) 1287–1299.
[24] O. Melchert, S. Willms, S. Bose, A. Yulin, B. Roth, F. Mitschke, U. Morgner, I. Babushkin, A. Demircan, Soliton molecules with two frequencies, Phys. Rev. Lett. 123 (2019) 243905.
[25] O. Melchert, S. Willms, U. Morgner, I. Babushkin, A. Demircan, Crossover from two-frequency pulse compounds to escaping solitons, Sci. Rep. 11 (2021) 11190.
[26] K.K.K. Tam, T.J. Alexander, A. Blanco-Redondo, C.M. de Sterke, Generalized dispersion Kerr solitons, Phys. Rev. A 101 (2020) 043822.
[27] J.P. Lourdesamy, A.F.J. Runge, T.J. Alexander, D.D. Hudson, A. Blanco-Redondo, C.M. de Sterke, Spectrally periodic pulses for enhancement of optical nonlinear effects, Nat. Phys. 18 (2021) 59–66.
[28] D. Mao, H. Wang, H. Zhang, C. Zeng, Y. Du, Z. He, Z. Sun, J. Zhao, Synchronized multi-wavelength soliton fiber laser via intracavity group delay modulation, Nature Commun. 12 (2021) 6712.
[29] Y. Cui, Y. Zhang, X. Yao, X. Hao, Q. Yang, D. Chen, X. Liu, X. Liu, B. Malomed, Dichromatic soliton-molecular compounds in synchronized mode-locked fiber lasers, 2022, preprint at https://arxiv.org/abs/2211.06061.
[30] O. Melchert, A. Demircan, Incoherent two-color pulse compounds, Opt. Lett. 46 (2021) 5603.
[31] S. Willms, O. Melchert, S. Bose, A. Yulin, I. Oreshnikov, U. Morgner, I. Babushkin, A. Demircan, Heteronuclear soliton molecules with two frequencies, Phys. Rev. A 105 (2022) 053525.
[32] J.P. Lourdesamy, J. Widjaja, G. Hawi, S. Kesarwani, A.F.J. Runge, C.M. de Sterke, Optimization of nonlinear enhancement through linear dispersion engineering, J. Opt. Soc. Amer. B 40 (2) (2023) 273–278.
[33] O. Melchert, A. Yulin, A. Demircan, Dynamics of localized dissipative structures in a generalized Lugiato–Lefever model with negative quartic group-velocity dispersion, Opt. Lett. 45 (2020) 2764.
[34] G. Moille, Q. Li, S. Kim, D. Westly, K. Srinivasan, Phased-locked two-color single soliton microcombs in dispersion-engineered Si3N4 resonators, Opt. Lett. 43 (2018) 2772–2775.
[35] M. Stratmann, T. Pagel, F. Mitschke, Experimental observation of temporal soliton molecules, Phys. Rev. Lett. 95 (2005) 143902.
[36] A. Hause, H. Hartwig, M. Böhm, F. Mitschke, Binding mechanism of temporal soliton molecules, Phys. Rev. A 78 (2008) 063817.
[37] E. Jones, T. Oliphant, P. Peterson, et al., SciPy: Open source scientific tools for Python, 2001–2018, http://www.scipy.org/ (Online; Accessed 09 March 2020).
[38] P. Virtanen, R. Gommers, T.E. Oliphant, et al., SciPy 1.0: Fundamental algorithms for scientific computing in Python, Nature Methods 17 (2020) 261.
[39] M.F. Saleh, F. Biancalana, Soliton-radiation trapping in gas-filled photonic crystal fibers, Phys. Rev. A 87 (2013) 043807.
[40] A.M. Heidt, Efficient adaptive step size method for the simulation of supercontinuum generation in optical fibers, J. Lightwave Tech. 27 (18) (2009) 3984.

[41] O. Melchert, A. Demircan, Py-fmas: A Python package for ultrashort optical pulse propagation in terms of forward models for the analytic signal, Comput. Phys. Comm. 273 (2022) 108257.
[42] W.H. Press, S.A. Teukolsky, W.T. Vetterling, B.P. Flannery, Numerical Recipes 3rd Edition: The Art of Scientific Computing, Cambridge University Press, USA, 2007.
[43] J. Weideman, B. Herbst, Split-step methods for the solution of the nonlinear Schrödinger equation, SIAM J. Numer. Anal. 23 (1986) 485.
[44] J. Hult, A fourth-order Runge–Kutta in the interaction picture method for simulating supercontinuum generation in optical fibers, J. Lightwave Tech. 25 (12) (2007) 3770.
[45] T. Taha, M. Ablowitz, Analytical and numerical aspects of certain nonlinear evolution equations. II. Numerical, nonlinear Schrödinger equation, J. Comput. Phys. 55 (1984) 203.
[46] P.L. DeVries, Application of the split operator Fourier transform method to the solution of the nonlinear Schrödinger equation, AIP Conf. Proc. 160 (1987) 269.
[47] O. Melchert, B. Roth, U. Morgner, A. Demircan, OptFROG — Analytic signal spectrograms with optimized time–frequency resolution, SoftwareX 10 (2019) 100275.
[48] L. Cohen, Time-frequency distributions – a review, Proc. IEEE 77 (1989) 941–981.
[49] J.M. Dudley, X. Gu, L. Xu, M. Kimmel, E. Zeek, P. O'Shea, R. Trebino, S. Coen, R.S. Windeler, Cross-correlation frequency resolved optical gating analysis of broadband continuum generation in photonic crystal fiber: Simulations and experiments, Opt. Express 10 (2002) 1215.
[50] N. Akhmediev, M. Karlsson, Cherenkov radiation emitted by solitons in optical fibers, Phys. Rev. A 51 (1995) 2602–2607.
[51] S. Pickartz, U. Bandelow, S. Amiranashvili, Adiabatic theory of solitons fed by dispersive waves, Phys. Rev. A 94 (2016) 033811.
[52] H.A. Haus, E.P. Ippen, Group velocity of solitons, Opt. Lett. 26 (2001) 1654–1656.
[53] J.P. Lourdesamy, J. Widjaja, G. Hawi, S. Kesarwani, A.F.J. Runge, C.M. de Sterke, Optimization of nonlinear enhancement through linear dispersion engineering, J. Opt. Soc. Amer. B 40 (2023) 273–278.
[54] O. Melchert, S. Bose, S. Willms, I. Babushkin, U. Morgner, A. Demircan, Two-color pulse compounds in waveguides with a zero-nonlinearity point, Opt. Lett. 48 (2023) 518–521.
[55] O. Melchert, S. Willms, I. Oreshnikov, A. Yulin, U. Morgner, I. Babushkin, A. Demircan, Resonant Kushi-comb-like multi-frequency radiation of oscillating two-color soliton molecules, New J. Phys. 25 (2023) 013003.
[56] T. Ueda, W.L. Kath, Dynamics of coupled solitons in nonlinear optical fibers, Phys. Rev. A 42 (1990) 563–571.
[57] C.R. Menyuk, Stability of solitons in birefringent optical fibers. II. Arbitrary amplitudes, J. Opt. Soc. Amer. B 5 (1988) 392–402.
[58] V.V. Afanasjev, E.M. Dianov, A.M. Prokhorov, V.N. Serkin, Nonlinear pairing of light and dark optical solitons, Pis'ma Zh. Eksp. Teor. Fiz. 48 (1988) 588.
[59] S. Trillo, S. Wabnitz, E.M. Wright, G.I. Stegeman, Optical solitary waves induced by cross-phase modulation, Opt. Lett. 13 (10) (1988) 871–873.
[60] V.V. Afanasyev, Y.S. Kivshar, V.V. Konotop, V.N. Serkin, Dynamics of coupled dark and bright optical solitons, Opt. Lett. 14 (15) (1989) 805–807.
[61] V.K. Mesentsev, S.K. Turitsyn, Stability of vector solitons in optical fibers, Opt. Lett. 17 (21) (1992) 1497–1499.
[62] N. Akhmediev, A. Ankiewicz, Multi-soliton complexes, Chaos 10 (3) (2000) 600–612.
[63] L.D. Landau, L.M. Lifshitz, Quantum Mechanics Non-Relativistic Theory, Vol. 3, Elsevier Science, Oxford, 1981.
[64] J. Lekner, Reflectionless eigenstates of the sech^2 potential, Amer. J. Phys. 75 (2007) 1151.
[65] M. Abramowitz, I.A. Stegun, Handbook of Mathematical Functions with Formulas, Graphs and Mathematical Tables, Dover, New York, 1972.
[66] O. Melchert, S. Willms, I. Babushkin, U. Morgner, A. Demircan, Two-color soliton meta-atoms and molecules: supplemental material, Zenodo, 2023, repository at http://dx.doi.org/10.5281/zenodo.7708414.
[67] P. Bocchieri, A. Loinger, Quantum recurrence theorem, Phys. Rev. 107 (1957) 337.
[68] D.F. Styer, Quantum revivals versus classical periodicity in the infinite square well, Amer. J. Phys. 69 (2001) 56–62.
[69] I. Babushkin, O. Melchert, U. Morgner, A. Demircan, Photon trapping in a time cavity flying with a speed of light, 2022, preprint at http://dx.doi.org/10.21203/rs.3.rs-1982423/v1.
[70] I. Oreshnikov, O. Melchert, S. Willms, S. Bose, I. Babushkin, A. Demircan, U. Morgner, A. Yulin, Cherenkov radiation and scattering of external dispersive waves by two-color solitons, Phys. Rev. A 106 (2022) 053514.
[71] M. Haelterman, A. Sheppard, A. Snyder, Bound-vector solitary waves in isotropic nonlinear dispersive media, Opt. Lett. 18 (1993) 1406.
[72] Y. Silberberg, Y. Barad, Rotating vector solitary waves in isotropic fibers, Opt. Lett. 20 (1995) 246.
[73] D. Pelinovsky, Y. Kivshar, Stability criterion for multicomponent solitary waves, Phys. Rev. E 62 (2000) 8668.
[74] C. Paré, Accurate variational approach for vector solitary waves, Phys. Rev. E 54 (1996) 846.
[75] Z. Musslimani, J. Yang, Self-trapping of light in a two-dimensional photonic lattice, J. Opt. Soc. Amer. B 21 (2004) 973.
[76] M. Ablowitz, Z. Musslimani, Spectral renormalization method for computing self-localized solutions to nonlinear systems, Opt. Lett. 30 (2005) 2140.
[77] G. Fibich, Y. Sivan, M. Weinstein, Bound states of nonlinear Schrödinger equations with a periodic nonlinear microstructure, Physica D 217 (2006) 31.
[78] T. Lakoba, J. Yang, A generalized Petviashvili iteration method for scalar and vector Hamiltonian equations with arbitrary form of nonlinearity, J. Comput. Phys. 226 (2007) 1668.
[79] J. Yang, T. Lakoba, Universally-convergent squared-operator iteration methods for solitary waves in general nonlinear wave equations, Stud. Appl. Math. 118 (2007) 153.
[80] T. Lakoba, Conjugate gradient method for finding fundamental solitary waves, Physica D 238 (2009) 2308.
[81] J. Yang, Newton-conjugate-gradient methods for solitary wave computations, J. Comput. Phys. 228 (2009) 7007.
[82] M. Chiofalo, S. Succi, M. Tosi, Ground state of trapped interacting Bose-Einstein condensates by an explicit imaginary-time algorithm, Phys. Rev. E 62 (2000) 7438.
[83] J. Yang, T. Lakoba, Accelerated imaginary-time evolution methods for the computation of solitary waves, Stud. Appl. Math. 120 (2008) 265.
[84] N. Dror, B. Malomed, Solitons and vortices in nonlinear potential wells, J. Opt. 18 (2016) 014003.
[85] J. Kierzenka, L. Shampine, A BVP solver based on residual control and the MATLAB PSE, ACM Trans. Math. Software 27 (2001) 300.
[86] M.V. Tratnik, J.E. Sipe, Bound solitary waves in a birefringent optical fiber, Phys. Rev. A 38 (1988) 2011–2017.
[87] D.N. Christodoulides, R.I. Joseph, Vector solitons in birefringent nonlinear dispersive media, Opt. Lett. 13 (1988) 53.
[88] Y.S. Kivshar, Soliton stability in birefringent optical fibers: Analytical approach, J. Opt. Soc. Amer. B (1990) 2204.
[89] M.V. Tratnik, Twisted solitons in birefingent optical fibers, Opt. Lett. 17 (1992) 917.
[90] V.V. Afanasjev, Soliton polarization rotation in fiber lasers, Opt. Lett. 20 (1995) 270.
[91] A.V. Yulin, D.V. Skryabin, P.S.J. Russell, Four-wave mixing of linear waves and solitons in fibers with higher-order dispersion, Opt. Lett. 29 (20) (2004) 2411–2413.
[92] D.V. Skryabin, A.V. Yulin, Theory of generation of new frequencies by mixing of solitons and dispersive waves in optical fibers, Phys. Rev. E 72 (2005) 016619.
[93] M. Conforti, S. Trillo, A. Mussot, A. Kudlinski, Parametric excitation of multiple resonant radiations from localized wavepackets, Sci. Rep. 5 (2015) 9433.
[94] I. Oreshnikov, R. Driben, A. Yulin, Dispersive radiation and regime switching of oscillating bound solitons in twin-core fibers near zero-dispersion wavelength, Phys. Rev. A 96 (2017) 013809.
[95] O. Melchert, A. Demircan, A. Yulin, Multi-frequency radiation of dissipative solitons in optical fiber cavities, Sci. Rep. 10 (2020) 8849.

[96] R. Driben, A. Husakou, J. Herrmann, Low-threshold supercontinuum generation in glasses doped with silver nanoparticles, Opt. Express 17 (2009) 17989–17995.
[97] S. Bose, R. Chattopadhyay, S. Roy, S.K. Bhadra, Study of nonlinear dynamics in silver-nanoparticle-doped photonic crystal fiber, J. Opt. Soc. Amer. B 33 (2016) 1014–1021.
[98] S. Bose, A. Sahoo, R. Chattopadhyay, S. Roy, S.K. Bhadra, G.P. Agrawal, Implications of a zero-nonlinearity wavelength in photonic crystal fibers doped with silver nanoparticles, Phys. Rev. A 94 (2016) 043835.
[99] F.R. Arteaga-Sierra, A. Antikainen, G.P. Agrawal, Soliton dynamics in photonic-crystal fibers with frequency-dependent Kerr nonlinearity, Phys. Rev. A 98 (2018) 013830.
[100] S. Zhao, R. Guo, Y. Zeng, Effects of frequency-dependent Kerr nonlinearity on higher-order soliton evolution in a photonic crystal fiber with one zero-dispersion wavelength, Phys. Rev. A 106 (2022) 033516.